A Hybrid Dynamic Model Of An Insect-Like MAV With Soft Wings

Ayman Belkhiri, Mathieu Porez, Frédéric Boyer

A Hybrid Dynamic Model Of An Insect-Like MAV With Soft Wings

Ayman Belkhiri[1], Mathieu Porez[1] and Frédéric Boyer[1]

***Abstract*— This paper presents a hybrid dynamic model of a 3-D aerial insect-like robot. The soft-bodied insect wings modeling is based on a continuous version of the Newton-Euler dynamics where the leading edge is treated as a continuous Cosserat beam. These wings are connected to an insect's rigid thorax using a discrete recursive algorithm based on the Newton-Euler equations. Here we detail the inverse dynamic model algorithm. This version of the dynamic model solves the following two problems involved in any locomotion task: 1°) it enables the net motion of a reference body to be computed from the known data of internal motions (strain fields); 2°) it gives the internal torques required to impose these internal (strain fields) motions. The essential fluid effects have been taken into account using a simplified analytical hovering flight aerodynamic model. To facilitate the analysis of numerical results, a visualization tool is developed (see video available at [1]).**

I. INTRODUCTION

Biologically inspired Micro Aerial Vehicles (MAVs) have the potential to fly, maneuver, collect information and act in Dull - Dirty - Dangerous environments. In the last decade, the number of researches related to MAVs has exploded and many successful prototypes and designs exist now. The vast majority of these research activities deals with : aerodynamic, fluid-structure interactions, prototyping and control problems. It should be noted that in these works there are two main categories of dynamic models. The first ones are finite elements based models coupled with CFD solvers [2], [3], [4]. These models are accurate but they need heavy computations. In the other hand, the second category uses very simple dynamical models [5], [6], [7], [8]. This kind of models is suitable for control and real time applications, however, it does not take into account the flexibility of the wings which is a key parameter for insect-like flapping flight. In an attempt to start overcoming these modeling deficiencies, we propose in this paper a dynamic model where the insect's thorax is considered as a rigid body connected with two soft wings. The proposed model is aiming to replicate as closely as possible the kinematics and internal deformations of the wing as well as the rigid net motion of the insect. The proposed model is distinguished by the following two points: 1°) it is a dynamic model called "hybrid", combining discrete and continuous models taking into account the wing bending and twisting deformations as well as the external aerodynamic forces; 2°) the computational efficiency of the proposed algorithms and the highly realistic visual rendering of the simulations (see video in [1]) allow one to access many information that were, until now, unreachable e.g. the internal torques, the aerodynamic forces, the wing-thorax reaction torques, the passivity of the wings, etc.

The paper is organized as follows. We start first by recalling the general modeling framework along with some basic notations and mathematical definitions. Then, we expose our hybrid dynamic model starting by discrete insect's body model. Then, we detail the continuous wing model followed by the aerodynamic model. After that, we expose the general algorithm that allows one to establish the connection between the different insect's parts. We explain how we can establish the connection between the thorax and the wing's models and how to mix them to form a 'hybrid' algorithm modeling the hole insect. The obtained algorithm will perform fast calculations of the control torques exerted at the thorax-wing junction as well as those applied along the leading edge span. Moreover, it will compute the overall rigid (net) motions involved in locomotion tasks. Finally we present some examples of simulations and results. The paper ends with some concluding remarks.

[1]All the authors are with IRCCyN laboratory and Ecole des Mines de Nantes, 4, rue Alfred Kastler, B.P. 20722, F-44307, Nantes Cedex 3, France. E-mails: ayman.belkhiri at mines-nantes.fr, mathieu.porez at mines-nantes.fr, frederic.boyer at mines-nantes.fr.

II. MODELING APPROACH

To model our bio-inspired insect-like robot, we consider it as an assembly of three distinct bodies i.e. a thorax and two wings forming a tree-like structure completely disconnected from the earth. In this regard, let us highlight two essential points: 1°) Globally, the insect can be considered as an "unconstrained mobile multibody system". To establish the dynamic locomotion model of such kind of systems, Boyer *et al.* [9] proposed a unified computational method based on Newton-Euler (N-E) formulation to model a wide range of discrete mobile multibody systems including bio-inspired snake-like robots, swimming eel-like robots, flying insect-like robots, etc. 2°) However, when dealing with the wings, the number of internal degree of freedom of each wing tends to infinity. Thus, the wing becomes a 'continuous-like system' and the discrete mobile multibody systems approach is no longer valid in that case. To skirt this problem, Boyer *et al.* [10] proposed a continuous version of the Newton-Euler discrete algorithm in which the bio-inspired robot is modeled as a geometrically exact beam continuously actuated through an active strain law. Hence, to address the insect-like dynamic locomotion problem accurately we need to consider both of these approaches: 1°) the discrete one for the thorax; 2°) the continuous one for the wings.

III. INSECT DYNAMIC MODELING

A. Description of the insect

In acordance with Fig.1, let us consider an insect-like robot S_o^+ composed by a thorax S_o and two wings S_1 and S_2, the right and left one respectively. Each wing is connected to the thorax through an actuated revolute joint. We attach to the ambient geometric space a fixed orthonormal frame denoted by $\mathcal{F}_e = (O, e_x, e_y, e_z)$ and to each link S_j an orthonormal mobile frame $\mathcal{F}_j = (O_j, s_j, n_j, a_j)$ for $j = 0, 1, 2$. At any time t, the robot configuration is defined by the joint positions r, the wing strains (see section IV for more details) and the rigid transformation ${}^e g_o$ of $\mathcal{F}_o$ with respect to $\mathcal{F}_e$. Let us note that we chose S_o as the reference of the net motions of our virtual insect-like robot. In this section, following usual N-E conventions of the multi-body system modeling and labeling (see [11]), we reserve the subscript 0 for the thorax, the subscript 1 for the right wing and the subscript 2 for the left wing. Let us start by introducing the

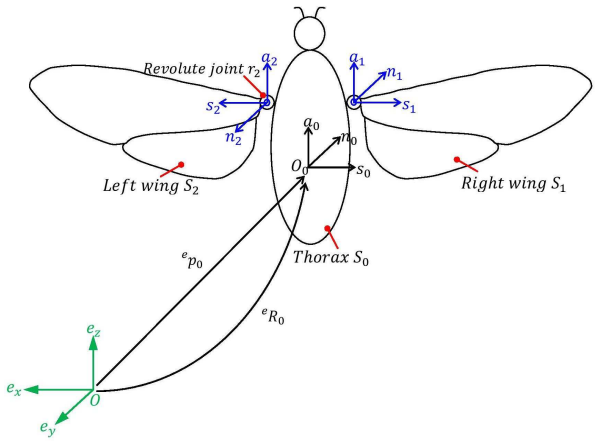

Fig. 1: Frames and parametrization of the insect-like MAV.

geometric model of the robot. For links $j = 1, 2$, the rigid transformation (elements of SE(3)), which define the posture of the frame $\mathcal{F}_j$ with respect to the frame $\mathcal{F}_e$ is described by:

$$ {}^e g_j = {}^e g_o \, {}^o g_j(r_j) \text{ , with } {}^o g_j(r_j) = \begin{pmatrix} {}^o R_j(r_j) & {}^o P_j \\ 0 & 1 \end{pmatrix} , \quad (1) $$

where ${}^o R_j$ and ${}^o P_j$ are the orientation matrix and the position vector of $\mathcal{F}_j$ with respect to $\mathcal{F}_o$ respectively. The twist of the link j denoted by η_j is defined by a (6×1) vector of link velocity components expressed in $\mathcal{F}_j$, i.e.:

$$ \eta_j = (V_j^T, \Omega_j^T)^T = Ad_{{}^j g_o} \eta_o + \dot{r}_j A_j , \quad (2) $$

where V_j and Ω_j are respectively the linear and angular Galilean velocities of the considered link, $A_j = (0_3^T, a_j^T)^T$ is the unit vector representing the joint axis j, and $Ad_{{}^j g_o}$ is the adjoint map operator (see appendix). Once the Galilean velocities are defined, by temporal derivation of (2), the accelerations denoted by $\dot{\eta}_j$ of the link j become:

$$ \dot{\eta}_j = Ad_{{}^j g_o} \dot{\eta}_o + \zeta_j(\dot{r}_j, \ddot{r}_j) , \quad (3) $$

where ζ_j represents the part of accelerations that do not depend of the thorax accelerations. ζ_j has the following form:

$$ \zeta_j = \begin{pmatrix} ({}^j V_o + {}^j P_o \times {}^j \Omega_o) \times \dot{r}_j a_j \\ {}^j \Omega_o \times \dot{r}_j a_j \end{pmatrix} + \ddot{r}_j A_j . \quad (4) $$

Finally, by applying, on each body, the Newton's law and the Euler's theorem, the dynamic equations of links from S_o to S_2 are:

$$ 0 = \mathcal{M}_o \dot{\eta}_o + F_{gyr,o} - F_{ext,o} + \sum_{j=1}^{j=2} Ad^*_{{}^j g_o} F_j , \quad (5) $$

$$ F_1 = \mathcal{M}_1 \dot{\eta}_1 + F_{gyr,1} - F_{ext,1} \text{ , and} \quad (6) $$

$$ F_2 = \mathcal{M}_2 \dot{\eta}_2 + F_{gyr,2} - F_{ext,2} , \quad (7) $$

where, from left to right, we introduce the following physical variables:

- the wrench of joint forces denoted by F_j exerted by the link 0 on the link j;
- the j^{th} body inertia tensor denoted by $\mathcal{M}_j$ and defined by the following equation[1]:

$$ \mathcal{M}_j = \begin{pmatrix} m_j 1_3 & -\hat{m} s_j \\ \hat{m} s_j & I_j \end{pmatrix} , \quad (8) $$

where m_j, ms_j and I_j are the mass, the first moment vector and the inertia tensor of the link j respectively;

- the wrench of gyroscopic forces applied on the link j:

$$ F_{gyr,j} = \begin{pmatrix} \Omega_j \times (\Omega_j \times m_j s_j) + \Omega_j \times m_j V_j \\ \Omega_j \times (I_j \Omega_j) + m_j s_j \times (\Omega_j \times V_j) \end{pmatrix} , \quad (9) $$

- the wrench of external forces denoted by $F_{ext,j}$ is defined in section V.

B. Forward dynamic model of MAV

In order to compute the net motion of the considered robot, we need to establish the forward dynamic model of this one, i.e the dynamic equations of the multi-body system S_o^+. From (5)-(7), the equation setting the external degrees of freedom of S_o^+ and describing the net motion of the robot is:

$$ \mathcal{M}_o^+(r(t)) \dot{\eta}_o = F_o^+(r(t), \dot{r}(t), \ddot{r}(t), {}^e g_o, \eta_o) , \quad (10) $$

where $\dot{\eta}_o$ is the accelerations of S_o and those of S_o^+, $\mathcal{M}_o^+$ is the generalized inertia matrix of S_o^+. It is given by:

$$ \mathcal{M}_o^+ = \sum_{j=0}^{j=2} Ad^*_{{}^j g_o} \mathcal{M}_j Ad_{{}^j g_o} . \quad (11) $$

$F_o^+(r(t), \dot{r}(t), \ddot{r}(t), {}^e g_o, \eta_o)$ is the wrench of all inertial and external forces and moments exerted onto S_o^+, i.e. :

$$ F_o^+ = F_{ext,o} - F_{gyr,o} + \sum_{j=1}^{j=2} Ad^*_{{}^j g_o} (F_{ext,j} - F_{gyr,j} - \mathcal{M}_j \zeta_j) . \quad (12) $$

Let us note that, in (12), $F_{gyr,o}$ is calculated directly using eq. (9), while $F_{gyr,1}$ and $F_{gyr,2}$ are obtained from the continuous dynamic model (see section IV-B). Moreover, for

[1] Let us note that for any vectors A and B in $\mathbb{R}^3$, $\hat{A}$ is defined such that $\hat{A}B = A \times B$.

the sake of simplicity, the aerodynamic wrench acting on the thorax $F_{ext,o}$ is neglected in this study. However, the calculus of the aerodynamic forces wrenches applied onto the right and left wings $F_{ext,1}$ and $F_{ext,2}$ is detailed in section V.

IV. WING DYNAMIC MODELING

To model the compliant wings of the insect and to compute the different physical variables related to these one (see (10)), we adopted the macro-continuous approach proposed by Boyer *et al.* in [10],[12]. This approach is suitable for modeling hyper-redundant robot involving a lot of DoFs. For the sake of simplicity of analysis, we make the choice of considering that each "hyper-redundant wing" is composed of a leading edge and a membrane without venation. In agreement with [13], the leading edge may be assimilated to a Cosserat beam or geometrically exact beam. In such theory, the beam is subject to finite 3-D transformations and small strains. Each cross-section of the beam (of span denoted by l) is rigid and is labeled by its abscissa X along the leading edge starting from the wing root. The reference configuration is considered to be straight and aligned with (O, s_j) (see Fig. 3). Moreover, for a given cross section X, we attach a non deformable membrane segment such that the leading edge undergoes flexion and torsion deformations while the membrane follows rigidly its motion.

A. Additional notations and definitions

To each X cross section, we attache a mobile orthonormal frame $\mathcal{F}_m(X,t) = (P, s, n, a)(X,t)$ such that: 1°) $P(X,t)$ coincides with the center of the cross section, 2°) the vector $s(X,t)$ is tangent to the centroidal line of the leading edge, 3°) the vector $a(X,t)$ is tangent to the wing membrane. The posture of the cross section X with respect to the frame $\mathcal{F}_e$ is given by:

$$g = \begin{pmatrix} R(X) & P(X) \\ 0 & 1 \end{pmatrix} . \tag{13}$$

On the leading edge, we defined two vector fields. The first is the time-twist field[2]:

$$\hat{\eta} : X \in [0,l] \mapsto \hat{\eta}(X,t) = g^{-1}\dot{g} \in se(3) , \tag{14}$$

where $\eta(X,t)$ defines the infinitesimal transformation undergone by the cross section X between two infinitely close instants t and $t+dt$. The second is the space-twist field such that:

$$\hat{\xi} : X \in [0,l] \mapsto \hat{\xi}(X,t) = g^{-1}g' \in se(3) , \tag{15}$$

where $\xi(X,t)$ defines the infinitesimal transformation undergone by the cross section X at fixed time t when the material axis slides from X to $X+dX$. Now, to 'copy' the flapping wing kinematics and deformations, we identify $\hat{\xi}$ to a desired control field explicitly dependent on the time and

[2]Let us note that for any $\zeta = (A^T, B^T)^T \in \mathbb{R}^6$ with $A \in \mathbb{R}^3$ and $B \in \mathbb{R}^3$, $\hat{\zeta} = \begin{pmatrix} \hat{B} & A \\ 0 & 0 \end{pmatrix}$.

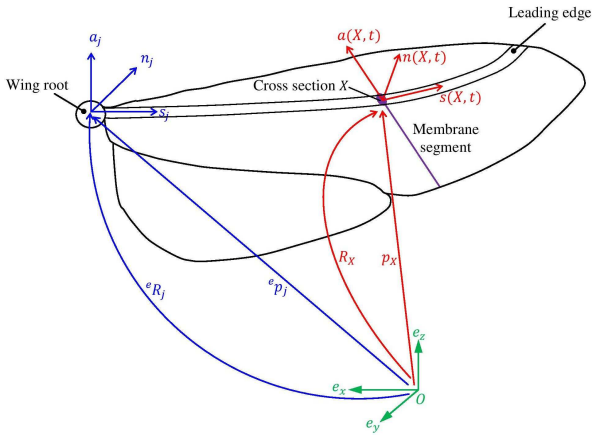

Fig. 3: Frames and parametrization of the soft wing.

noted $\hat{\xi}_d(X,t)$ which parameterizes the internal kinematics of the wing motion, i.e.:

$$g^{-1}g' = \begin{pmatrix} \widehat{K}_d(X,t) & \Gamma_d(X,t) \\ 0 & 0 \end{pmatrix} = \widehat{\xi}_d(X,t) , \tag{16}$$

where $K_d = (K_{dX}, K_{dY}, K_{dZ})$ and $\Gamma_d = (\Gamma_{dX}, \Gamma_{dY}, \Gamma_{dZ})$. The K_{dX} component is the rate of twist per unit of wing span. It represents the torsion of the wing around its leading edge. The K_{dZ} and K_{dY} components are the curvatures of its centroidal line in the planes (P,s,n) and (P,a,s) respectively. The first one represent the flexion of the wing in the stroke plane, while the second one, represents the azimuthal or the elevation curvature. In the same way, $(\Gamma_{dX} - 1)$ is the rate of stretching of the centroidal line. Since the leading edge is inextensible, Γ_{dX} is set to 1 (see [10]). Γ_{dY} and Γ_{dZ} are the local transverse shearing rotations around the axes (P,a) and (P,n) respectively and they are equal to zero.

B. Continuous model of wings

Let us note that the macro-continuous framework used here is nothing else but a continuous version of the discrete framework presented in the section III, where the Cosserat beam stands for the mobile multibody system, a beam cross section stands for a discrete body, and finally the strain field ξ stands for the joint coordinates r. Pushing forward the analogy, each one of the wings will need a reference body (i.e. a reference cross section). In this case, we naturally chose the root, i.e the cross section labeled by $X = 0$ as a reference for the wing modeling. The continuous kinematic model of the wing splits into 3 equations detailed as follows:

- *Continuous model of transformations:* this is immediately derived from the definition (16) of internal DoFs:

$$g' = g\hat{\xi}_d(t), \text{ with } g(X=0) = {}^eg_j . \tag{17}$$

The boundary condition of (17) is determined by (1).

- *Continuous model of velocities:* by taking the derivative of (14) with respect to X, and by invoking (16) and the ad

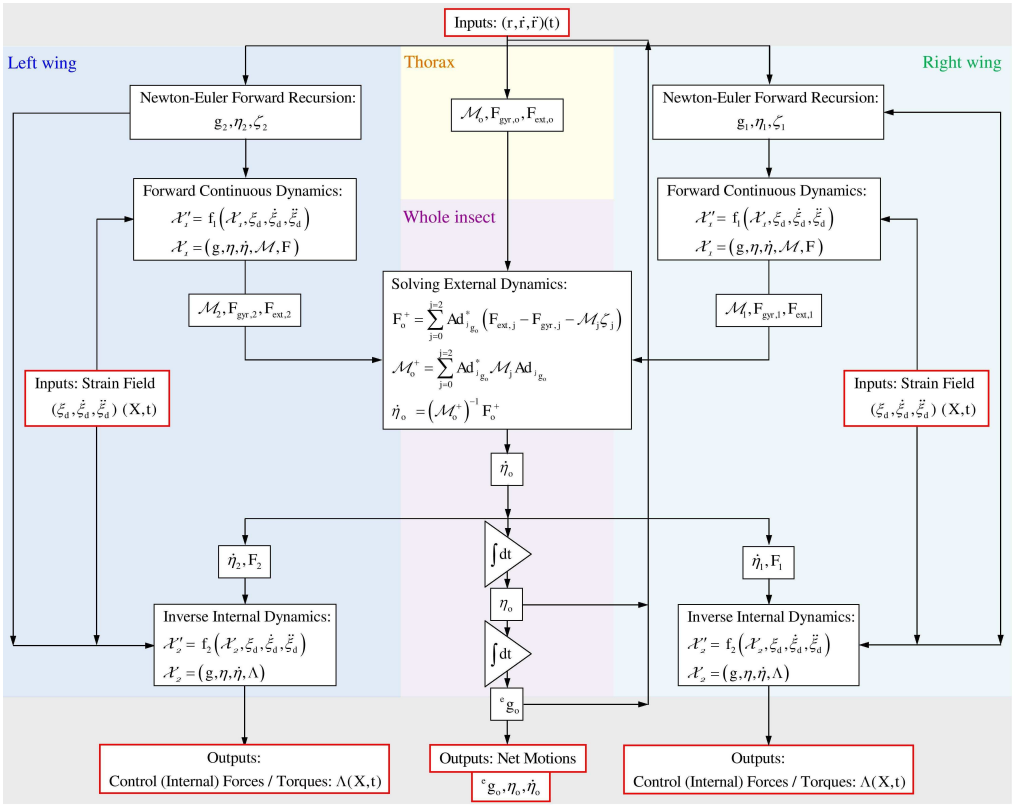

Fig. 2: Working schematic of the 'hybrid' locomotion dynamic model of insect-like MAV with soft wings.

operator (see appendix), we obtain:

$$\eta' = -ad_{\xi_d(t)}(\eta) + \dot{\xi}_d(t), \text{ with } \eta(X=0) = \eta_j. \quad (18)$$

At each time step, the thorax-wing junction point is animated by the velocity of the joint's flapping movement fed by the rigid net motion of the thorax. Hence the boundary conditions are obtained using (2).

• *Continuous model of accelerations:* this is inferred by taking the derivative of the previous model (18) with respect to time:

$$\dot{\eta}' = -ad_{\xi_d(t)}(\dot{\eta}) - ad_{\dot{\xi}_d(t)}(\eta) + \ddot{\xi}_d(t) \ , \quad (19)$$

with the boundary condition $\dot{\eta}(X=0) = \dot{\eta}_j$ fixed by (3).

Following the works detailed in [14], by applying the Hamilton principle on the wing subject to a density of imposed external (here aerodynamic) wrenches per unit of wing span $\overline{F}$ on $]0, l[$ and two punctual external wrenches F_- and F_+ imposed on $X=0$ and $X=l$ respectively, one obtains the following Partial Differential Equations (PDE) governing the dynamics of a wing cross section:

$$\mathcal{M}\dot{\eta} - ad^*_{\eta}(\mathcal{M}\eta) - \Lambda' + ad^*_{\xi_d(t)}(\Lambda) = \overline{F} \ , \quad (20)$$

with the boundary conditions:

$$\Lambda(0) = -F_- \ , \text{ and: } \Lambda(l) = F_+ \ , \quad (21)$$

where Λ is the density of internal wrenches ensuring the forcing of the internal desired strain: $\xi = \xi_d(t)$. Since the wings and the thorax are connected through joints, and they are mutually applying action and reaction forces on each other, the internal torques equation (20) is initialized by the thorax-wing reaction wrench calculated using (6) for S_1 and (7) for S_2. Finally the boundary conditions (21) become (for $j = 1, 2$):

$$\Lambda(0) = F_j = \mathcal{M}_j\dot{\eta}_j - F_{ext,j} + F_{gyr,j} \ , \quad (22)$$

$$\Lambda(l) = 0 \ , \quad (23)$$

where, $\mathcal{M}_j$ and $F_{gyr,j}$ stand for the inertia tensor and the inertial wrenches of the whole wing, both reduced to the reference cross section $X=0$, while $F_{ext,j}$ stands for the wing external aerodynamic forces wrench reduced to the reference cross section $X=0$ (see section V). We define $\mathcal{M}_j$ by:

$$\mathcal{M}_j = \int_0^l Ad_k^* \mathcal{M} Ad_k dX \ , \quad (24)$$

where, $\mathcal{M}$ is the inertia matrix of the cross section X connected to its membrane segment. The external wrenches, reduced to the reference cross section (i.e. the thorax-wing junction) are equal to:

$$F_{ext,j} = -F_- + Ad^*_{k_+}F_+ + \int_0^l Ad_k^*(\overline{F})dX \ , \quad (25)$$

and the inertial wrenches reduced to the reference cross

section are given by:

$$F_{gyr,j} = \int_0^l Ad_k^*(\mathcal{M}\zeta - ad_\eta^*(\mathcal{M}\eta))dX \ . \qquad (26)$$

V. Aerodynamic model

As a reminder, (10) rules the forward dynamics by computing the net accelerations from a model of external forces: the aerodynamic loads. In general, due to the complex topology of the flow surrounding a flapping wing, such a model requires the computation of the Navier-Stokes equations (see [2], [3], [15]). However, for prototyping and control-oriented applications, we have chosen to use a simplified analytical model based on the works of Dickinson *et al* [16], [17]. Dickinson's model was initially established using a dynamically scaled rigid wing model of fruit flies. Hence, we have rewritten these aerodynamic components in order to make them compatible with the "slice by slice" (cross-section by cross-section) formulation of our wing modeling strategy. For our simulations we select the following main aerodynamic contributions:

• *Stationary component*: Aerodynamically speaking, we define as stationary the effects that do not involve the derivatives of the angles of the wing movement. We typically meet these effects on a fixed airfoil in the presence of a steady flow: $\overline{F}_{stat} = \frac{1}{2}\,\rho\, c_X\, |\eta|^2\, C_{stat}$, where, C_{stat} denotes the (3×1) vector of stationary coefficients, ρ stands for the air density, and c_X represents the cord length at a given cross section X (for more details see [16]).

• *Rotational circulation*: It was shown that the rapid rotation of the wing during each change of direction causes a circulation of the air in the opposite direction, which increases the lift: $\overline{F}_{rot} = \rho\, c_X^2\, |\eta|\, C_{rot}\, \Omega$, where, C_{rot} denotes the (3×3) diagonal matrix of theoretical values of rotational coefficients (see [18], [17]).

• *Added mass*: The effect of the added mass is defined as the reaction due to the acceleration of the mass of fluid surrounding the wing, whose modeling is given here by: $\overline{F}_{add} = \partial(\mathcal{M}_{add}.\eta)/\partial t$, where $\mathcal{M}_{add}$ represents the (6×6) 'added inertia' matrix (see [19], [20]).

Let us remark that all the aerodynamic contributions are calculated in a frame attached to the aerodynamic center of each membrane segment. In order to include their effects on the insect dynamics, they must be transported to the cross-sectional frame $\mathcal{F}_m(X,t)$ using the appropriate adjoint map operator $Ad_{^a g_X}$, where ${}^a g_X$ stands for the homogeneous transformation matrix that defines the mapping between the frame attached to the aerodynamic center and the corresponding cross-sectional frame. Hence, the density of external aerodynamic wrenches per unit of span is defined by:

$$\overline{F} = Ad_{^a g_X}^*(\overline{F}_{stat} + \overline{F}_{rot} + \overline{F}_{add}) \ . \qquad (27)$$

Finally, from a qualitative viewpoint, these three components introduced in (27) are sufficient to reproduce the commonly observed aerodynamic phenomena during insect-like flapping flight. Moreover, by virtue of the intrinsic form of equation (25), one can enrich this model by adding other aerodynamic components e.g. wake capture, dynamic stall, transversal flow components, etc.

VI. General mixed continuous-discrete algorithm

From section II to section V we detailed the 'hybrid' dynamic model of a flapping wing MAV. The execution of the algorithm solving this model can be stated as follows. In accordance to Fig. 2, and at each time step of a global time loop:

1°) knowing the imposed time-dependant flapping kinematics $(r,\ \dot{r},\ \ddot{r})(t)$ and the internal strain law $(\xi_d,\ \dot{\xi}_d,\ \ddot{\xi}_d)(X,t)$, and using the forward discrete geometric model (1)-(3), we can compute the state of each thorax-wing junction point (g_j, η_j, ζ_j). This thorax-wing junction point state is used to initialize the first spatial integration loop of the forward continuous kinematic model i.e. (17)-(19). At the end of this integration, we recover the whole wing inertia tensor $\mathcal{M}_j$, the wrench of gyroscopic forces $F_{gyr,j}$ and the wrench of aerodynamic force $F_{ext,j}$ using (24), (26) and (25), respectively. At this stage, the algorithm is able to compute the generalized inertia matrix $\mathcal{M}_o^+$ and the wrench of all the inertial and external forces acting on the insect F_o^+ (see (11),(12)). Hence, the external dynamics are resolved and the thorax acceleration $\dot{\eta}_o$ is obtained using the dynamic equation of the whole insect (10).

2°) To compute the field of internal torques and forces along the wing span, we use the obtained $\dot{\eta}_o$ to calculate the thorax-wings reaction torques using equations (6) and (7). These reaction torques will determine the boundary conditions (22) initializing the second spatial integration loop (20).

3°) Since both external and internal dynamics are resolved, we can finally integrate the thorax acceleration $\dot{\eta}_o$ twice with respect to time to obtain the net motion of the whole insect: ${}^e g_o, \eta_o, \dot{\eta}_o$. This thorax state will be used to start the next time step of the global temporal integration loop.

VII. Illustrative examples and numerical results

In this section, we present some numerical results obtained using the hybrid algorithm presented in section VI. The simulation parameters were chosen such that the simulated MAV emulates as close as possible a real hawk moth (*Manduca sexta*). Hence, to approximate the moth we took the morphological parameters provided by [5]. The thorax is considered as an ellipsoid of great and small axis lengths $a = 40$ mm and $b = c = 10$ mm respectively. The wing span l is about 55 mm, whereas the maximum chord length is $c_{max} = 30$ mm. The mass of the MAV is $m = 1.8$ g where the wings represent approximatively 10% of the total weight of the MAV. The different kinematics of real *Manduca sexta* where measured experimentally by [21] and represented as a third order Fourier series. These kinematics were simplified and approximated by a first order

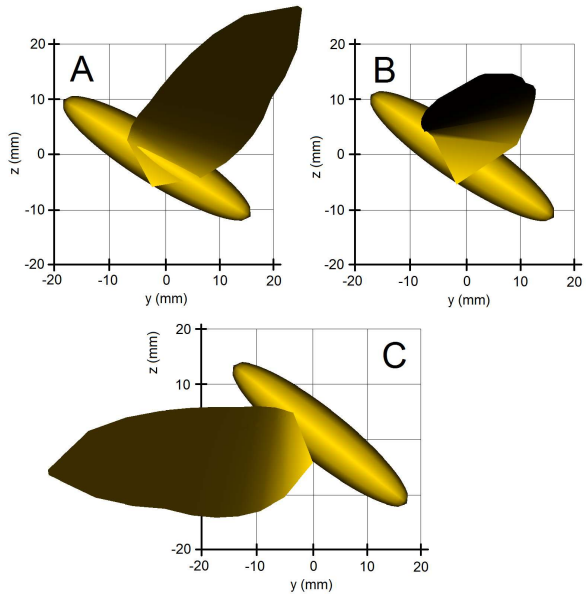

Fig. 4: Three snapshots during one flapping cycle: (a) beginning of the stroke, (b) middle of the stroke, (c) end of the stroke. The whole video sequence is available at:[1].

and symmetric Fourier series by [22]. Consequently, the time-dependant flapping law is: $r = r_o\ sin(\omega t)$, where $r_o = 60^o$ stands for the flapping amplitude and $\omega = 2\,\pi f$. Here, $f = 25$ Hz represents the flapping frequency [21]. The Reynolds number corresponding to these parameters is approximatively $R_e \simeq 10^4$. The spanwise wing torsion is introduced by the following strain law: $K_{dY} = K_{dZ} = 0$ and $K_{dX} = \alpha(X)h(t)$, where α is given in terms of X by: $\alpha = \alpha_1 - \alpha_1 e^{(-\alpha_2 X)}$, with α_1 and α_2 are positive constants. The time-dependant law $h(t)$ is given by: $h(t) = sin(\omega t - \phi)$ where ϕ represents the phase lag between the flapping $r(t)$ and torsion motions. The spanwise and chordwise flexion deformations are not considered in this simulation.

Due to the high number of parameters involved in this kind of simulations, it is important to have a visual feedback that facilitates the analysis of the numerical results. In Fig. 4, we show using VRML three snapshots taken at three different times during one flapping cycle. The position of the thorax S_o with respect to fixed frame $\mathcal{F}_e$ are reported in Fig. 5. As explained in section IV-B, the hybrid algorithm is able to evaluate the internal wrenches field along the wing span. The Fig. 6 illustrates an example of such computation at the middle and at the end of one flapping cycle. The time evolution of the lift generated by both wings of our MAV, as well as its aerodynamic components are represented in Fig. 7. The mean value of the total generated lift is $L = 3.2 \times 10^{-2}$ N. The hybrid algorithm allows one to gain insight into the interactions between the thorax and the wings through the computation of the thorax-wing reaction wrench (see Fig. 8).

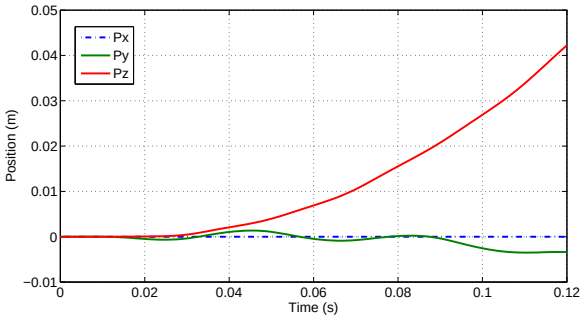

Fig. 5: Thorax position in the fixed frame.

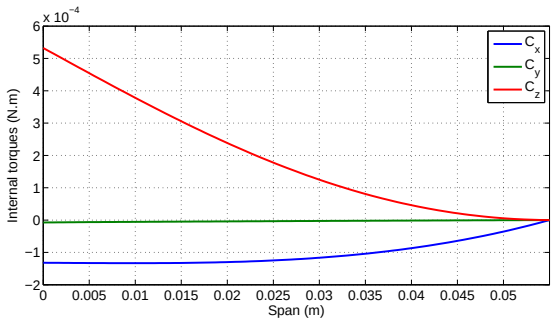

(a) Internal torques field at the middle of the stroke.

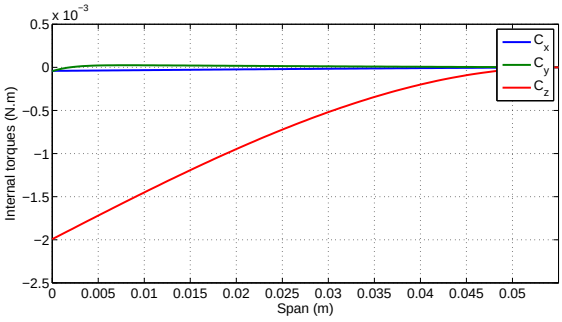

(b) Internal torques field at the end of the stroke.

Fig. 6: Internal torques field of the right wing.

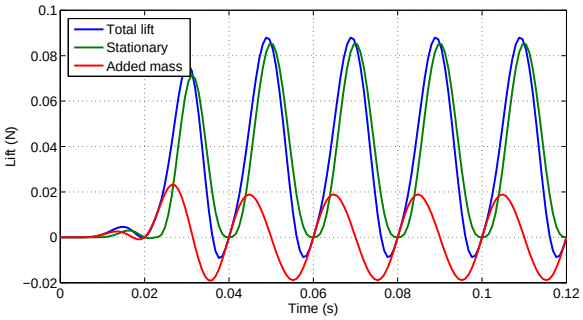

Fig. 7: The generated lift by one wing of the MAV.

VIII. CONCLUSIONS

In this paper, we presented a 'hybrid' dynamic model of an insect-like MAV. Contrary to previous works dealing with

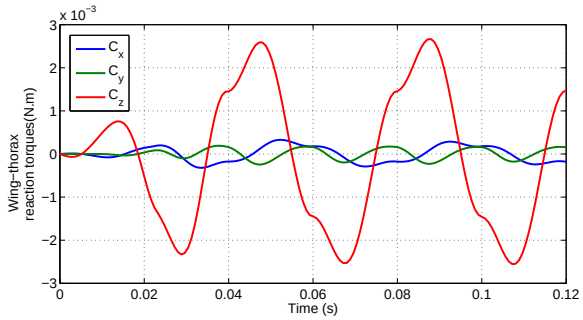

Fig. 8: Thorax-right wing reaction torques.

aerial robot modeling, our approach takes into account both the overall (net) motion of the insect as well as the wing's compliance. The wings are modeled using a continuous model based on a nonlinear beam. Moreover, based on the literature of air flow at low Reynolds number, a simplified analytical model is used to evaluate the aerodynamic performances of our aerial vehicle. To resolve the proposed locomotion model numerically, we developed a set of computationally efficient algorithms endowed with visual rendering routines. These developments could then constitute a 'generic tool' for soft wing MAVs modeling, design, prototyping and control-oriented applications. It could be also useful to investigate wing's elasticity and passivity problems using the imposed internal deformations and the calculated internal wrenches field. Hence, we could treat many problems of optimization and energetic efficiency frequently encountered in biology [23] and bio-inspired robotics.

APPENDIX

This appendix provides some basic insights of the notations of geometric mechanics [24]. The element $g \in SE(3)$ is a 4×4 homogeneous transformation matrix that defines the mapping between two frames:

$$g = \begin{pmatrix} R & p \\ 0 & 1 \end{pmatrix}. \tag{28}$$

Ad_g is a 6×6 matrix that once applied to a vector or twist changes it from one frame to another frame separated by transformation element g, where:

$$Ad_g = \begin{pmatrix} R & -R\,\hat{p} \\ 0 & R \end{pmatrix}. \tag{29}$$

For a given $\eta = (V^T, \Omega^T)^T \in \mathbb{R}^6$, ad_η is a 6×6 matrix that once applied to a vector (or twist), changes it from one frame to another frame separated by the infinitesimal transformation $(1 + \hat{\eta})$:

$$ad_\eta = \begin{pmatrix} \hat{\Omega} & \hat{V} \\ 0 & \hat{\Omega} \end{pmatrix}. \tag{30}$$

Passing to dual, Ad_g^* and ad_η^* define the 6×6 matrices that change any dual vector (or wrench) from one frame to another frame separated by g^T and $(1+\hat{\eta})^T$, respectively. Where, $Ad_g^* = Ad_g^T$ and $ad_\eta^* = ad_\eta^T$.

ACKNOWLEDGMENT

The authors would like to thank the French National Agency for Research (ANR) for supporting this work via EVA (Flying Autonomous Entomopter) project.

REFERENCES

[1] http://www.youtube.com/watch?v=dbG6gqNZRV8.

[2] H. Liu, "Integrated modeling of insect flight: From morphology, kinematics to aerodynamics," *Journal of Computational Physics*, vol. 228, no. 2, pp. 439–459, 2009.

[3] W. Shyy, H. Aono, S. K. Chimakurthi, P. Trizila, C. K. Kang, C. E. S. Cesnik, and H. Liu, "Recent progress in flapping wing aerodynamics and aeroelasticity," *Progress in Aerospace Sciences*, vol. 46, no. 7, pp. 284–327, 2010.

[4] P. Pai, D. Chernova, and A. Palazotto, "Nonlinear modeling and vibration characterization of mav flapping wings," *50th AIAA/ASME/ASCE/AHS/ASC Structures, Structural Dynamics, and Materials Conference*, pp. 1–25, 2009-2415.

[5] T. L. Hedrick and T. L. Daniel, "Flight control in the hawkmoth manduca sexta: The inverse problem of hovering," *Journal of Experimental Biology*, vol. 209, pp. 3114–3130, 2006.

[6] R. Zbikowski, S. Ansari, and K. Knowles, "On mathematical modelling of insect flight dynamics in the context of micro air vehicles," *Bioinspiration and Biomimetics*, vol. 1, no. 2, pp. R26–R36, 2006.

[7] N. Finio, B.M.and Perez-Arancibia and R. Wood, "System identification, modeling, and optimization of an insect-sized flapping-wing micro air vehicle," *2011 IEEE/RSJ International Conference on Intelligent Robots and Systems*, pp. 1107–1114, 2011.

[8] T. Rakotomamonjy, M. Ouladsine, and T. Le Moing, "Modelization and kinematics optimization for a flapping-wings microair vehicle," *Journal of Aircraft*, vol. 44, pp. 217–231, January-February 2007.

[9] F. Boyer and S. Ali, "Recursive inverse dynamics of mobile multibody systems with joints and wheels," *IEEE Transactions on Robotics*, vol. 27, pp. 215 – 228, April 2011.

[10] F. Boyer, S. Ali, and M. Porez, "Macro-continuous dynamics for hyper-redundant robots: Application to kinematic locomotion bio-inspired by elongated body animals," *IEEE Transactions on Robotics*, vol. 28, pp. 303 – 317, April 2012.

[11] W. Khalil and J.-F. Kleinfinger, "Minimum operations and minimum parameters of the dynamic models of tree structure robots," *IEEE Journal of Robotics and Automation*, vol. 3, pp. 517–526, December 1987.

[12] F. Boyer, M. Porez, and W. Khalil, "Macro-continuous computed torque algorithm for a three-dimensional eel-like robot," *IEEE Transactions on Robotics*, vol. 22, pp. 763–775, Aug. 2006.

[13] J. C. Simo and L. Vu-Quoc, "On the dynamics in space of rods undergoing large motions - A geometrically exact approach," *Computer Methods in Applied Mechanics and Engineering*, vol. 66, no. 2, pp. 125 – 161, 1988.

[14] F. Boyer, M. Porez, and A. Leroyer, "Poincaré-Cosserat equations for the Lighthill three-dimensional large amplitude elongated body theory: Application to robotics," *Journal of Nonlinear Science*, vol. 20, pp. 47–79, 2010.

[15] S. Ansari, R. Zbikowski, and K. Knowles, "Aerodynamic modelling of insect-like flapping flight for micro air vehicles," *Progress in Aerospace Sciences*, vol. 42, no. 2, pp. 129–172, 2006.

[16] M. H. Dickinson, F.-O. Lehmann, and S. P. Sane, "Wing rotation and the aerodynamic basis of insect flight," *Science*, vol. 284, no. 5422, pp. 1954–1960, 1999.

[17] J. A. Walker, "Rotational lift: Something different or more of the same?," *Journal of Experimental Biology*, vol. 205, pp. 3783–3792, 2002.

[18] S. P. Sane and M. Dickinson, "The aerodynamic effects of wing rotation and a revised quasi-steady model of flapping flight," *Journal of Experimental Biology*, vol. 205, pp. 1087–196, 2002.

[19] H. Lamb, *Hydrodynamics*. Cambridge University Press, 1932.

[20] J. D. DeLaurier, "An aerodynamic model for flapping-wing flight," *Aeronautical Journal*, pp. 125–130, April 1993.

[21] A. Willmott and C. Ellington, "The mechanics of flight in the hawkmoth manduca sexta. I. Kinematics of hovering and forward flight," *Journal of Experimental Biology*, vol. 200, pp. 2705–2722, 1997.

[22] S. Sane and M. Dickinson, "The control of flight force by a flapping wing: Lift and drag production," *Journal of Experimental Biology*, vol. 204, pp. 2607–2626, 2001.
[23] R. M. Alexander, *Elastic Mechanisms in Animal Movement*. Cambridge University Press, 1st ed., 1988.
[24] R. M. Murray, S. S. Sastry, and L. Zexiang, *A Mathematical Introduction to Robotic Manipulation*. Boca Raton, FL, USA: CRC Press, Inc., 1st ed., 1994.